How to cite: *Angew. Chem. Int. Ed.* **2023**, *62*, e202304465
doi.org/10.1002/anie.202304465

VIP Nanomedicine Very Important Paper

Integrated Cascade Nanozymes with Antisenescence Activities for Atherosclerosis Therapy

Wanling Liu[+], *Yihong Zhang*[+], *Gen Wei, Minxuan Zhang, Tong Li, Quanyi Liu, Zijun Zhou, Yan Du, and Hui Wei**

Abstract: Senescent cells are the critical drivers of atherosclerosis formation and maturation. Mitigating senescent cells holds promise for the treatment of atherosclerosis. In an atherosclerotic plaque microenvironment, senescent cells interact with reactive oxygen species (ROS), promoting the disease development. Here, we hypothesize that a cascade nanozyme with antisenescence and antioxidant activities can serve as an effective therapeutic for atherosclerosis. An integrated cascade nanozyme with superoxide dismutase- and glutathione peroxidase-like activities, named MSe_1, is developed in this work. The obtained cascade nanozyme can attenuate human umbilical vein endothelial cell (HUVEC) senescence by protecting DNA from damage. It significantly weakens inflammation in macrophages and HUVECs by eliminating overproduced intracellular ROS. Additionally, the MSe_1 nanozyme effectively inhibits foam cell formation in macrophages and HUVECs by decreasing the internalization of oxidized low-density lipoprotein. After intravenous administration, the MSe_1 nanozyme significantly inhibits the formation of atherosclerosis in apolipoprotein E-deficient ($ApoE^{-/-}$) mice by reducing oxidative stress and inflammation and then decreases the infiltration of inflammatory cells and senescent cells in atherosclerotic plaques. This study not only provides a cascade nanozyme but also suggests that the combination of antisenescence and antioxidative stress holds considerable promise for treating atherosclerosis.

Introduction

Cellular senescence is a state of irreversible cell cycle arrest associated with aging.[1] The senescent state can be induced by oxidative stress, metabolic dysfunction, and epigenetic regulation, among other stressors.[2] Senescent cells secrete inflammatory chemokines, cytokines, and reactive oxygen species (ROS),[3] leading to a series of specific changes in cell function[4] and consequently causing human aging and age-related vascular disorders. Recently, evidence linking senescent cells to atherosclerosis has emerged, revealing that senescent cells are vital drivers of atheroma formation and maturation.[5] The accumulation of senescent endothelial cells might cause inflammation and oxidative stress that impair endothelial function and stiffen large arteries, suggesting that cellular senescence *in vivo* contributes to the pathogenesis of human atherosclerosis.[6] With senescence, the antioxidant barrier changes. In senescent cells, the high level of ROS exhausts antioxidants, causing the failure of the antioxidant defense system.[7] During the progression of atherosclerosis, senescence accumulation and antioxidant enzyme subduction lead to pathologic remodeling of the vascular wall and eventually atherosclerosis.[8] This demonstrates the importance of supplying antioxidants as a therapeutic intervention against oxidative stress in senescent cells in atherosclerosis therapy. Normal vascular cells are equipped with a variety of antioxidant defense enzymes, including superoxide dismutase (SOD) and glutathione peroxidase (GPx), to mitigate oxidative stress and exert antiatherosclerosis effects. For example, SOD inhibits oxidative damage caused by superoxide radical ($O_2^{\bullet -}$).[9] Then, by reducing hydrogen peroxide (H_2O_2) to water and lipid hydroperoxides to their corresponding alcohols in mitochondria, GPx acts after SOD and is another primary antioxidant enzyme within vascular cells.[10] Notably, preclinical studies have shown that the deficiency of SOD and GPx

[*] W. Liu,[+] Y. Zhang,[+] G. Wei, M. Zhang, T. Li, Z. Zhou, Prof. Dr. H. Wei
College of Engineering and Applied Sciences, Nanjing National Laboratory of Microstructures, Jiangsu Key Laboratory of Artificial Functional Materials, Nanjing University
210023 Nanjing, Jiangsu (China)
E-mail: weihui@nju.edu.cn
Prof. Dr. H. Wei
State Key Laboratory of Analytical Chemistry for Life Science, School of Chemistry and Chemical Engineering, Chemistry and Biomedicine Innovation Center (ChemBIC), Nanjing University
210023 Nanjing, Jiangsu (China)
Q. Liu, Y. Du
State Key Laboratory of Electroanalytical Chemistry, Changchun Institute of Applied Chemistry, Chinese Academy of Sciences
130022 Jilin Changchun, (China)
and
School of Applied Chemistry and Engineering, University of Science and Technology of China
230026 Hefei, Anhui (China)
[+] These authors contributed equally to this work.

enhances atherosclerosis in apolipoprotein E-deficient ($ApoE^{-/-}$) mice, indicating the protective roles of SOD and GPx against atherogenesis.[11] Therefore, it is straightforward to use SOD and GPx as antioxidants for atherosclerosis therapy. Unfortunately, the low stability and high cost of natural enzymes make this approach very challenging. To tackle this challenge, we report an integrated cascade nanozyme with SOD- and GPx-like activities for atherosclerosis therapy by attenuating senescence and scavenging ROS.

Nanozymes, the emerging functional nanomaterials with enzyme-like activities, have shown promising applications in biomedicine.[12] In particular, antioxidative nanozymes with SOD-, catalase-, and GPx-like activities have been extensively explored for varieties of disease therapies.[13] One of the advantages of nanozymes over natural enzymes and conventional enzyme mimics is that they can rationally integrate multiple enzyme-like activities.[14] This superiority enables nanozymes to catalytically scavenge ROS in a cascade manner. For example, we have developed an integrated nanozyme with SOD- and catalase-like activities for cascade inflammatory bowel disease therapy.[15] Nevertheless, few efforts have been focused on atherosclerosis therapy by nanozymes themselves, especially cascade nanozymes.

Here, we fabricated MOF@Se nanozymes (MSe_1) with antisenescence and antioxidant capacities as therapeutic agents for alleviating atherosclerosis (Figure 1). MIL-53(Fe)-NO_2 MOF (MIL = Materials of Institute Lavoisier, MOF = metal–organic framework) had excellent SOD-like activity (Figure S1), which was confirmed through density functional theory calculations.[16] To endow the MIL-53(Fe)-NO_2 nanozyme with GPx-like activity, we doped it with selenium (Se), a key and essential trace element in the

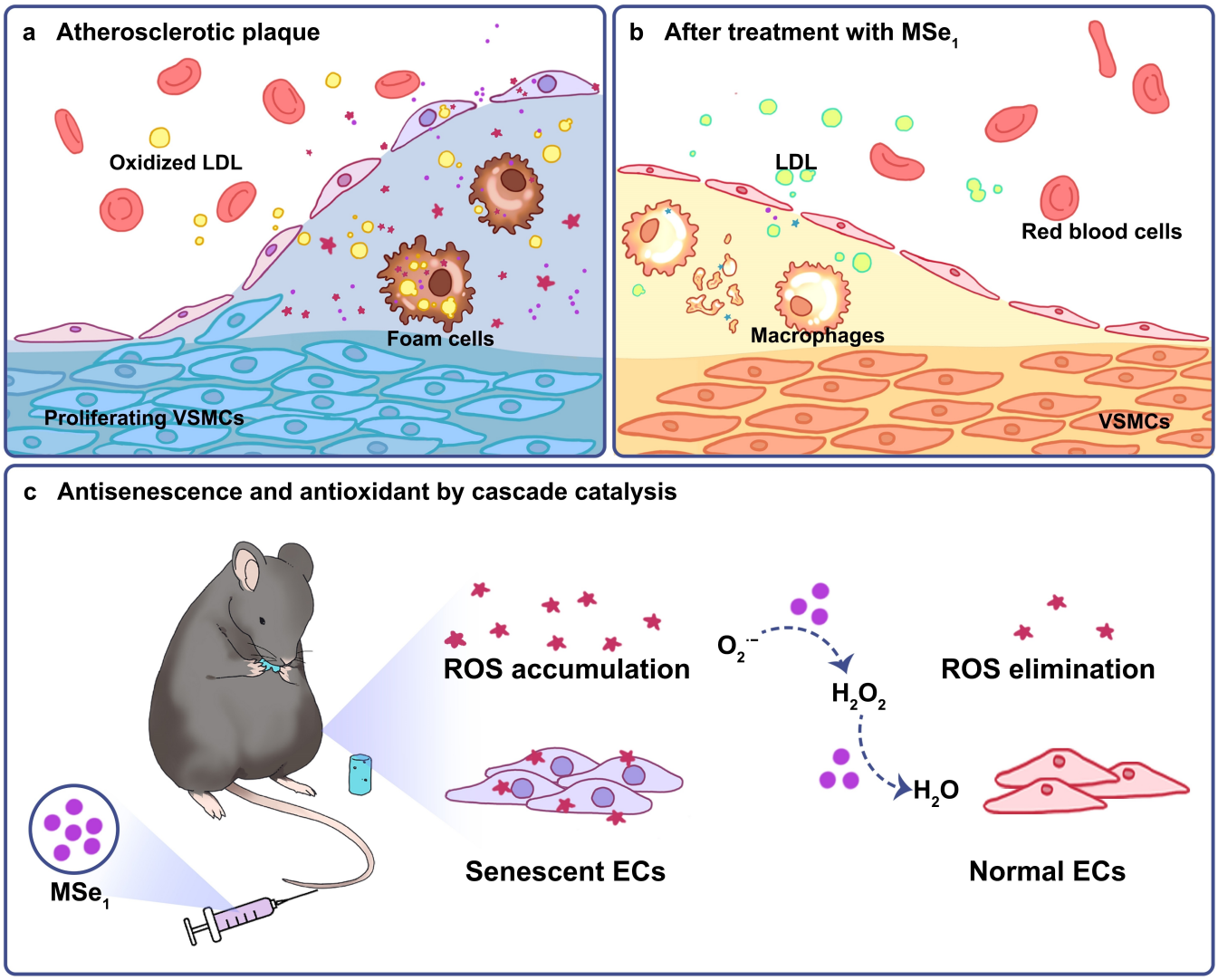

Figure 1. Schematic illustration of the MSe_1 cascade nanozyme with antisenescence and antioxidant activities for atherosclerosis therapy. a) Schematic illustrating a harmful atherosclerotic plaque microenvironment with senescent ECs, proliferated VSMCs, foam cells, and a high level of ROS. b) Atherosclerosis can be effectively relieved through treatment with the MSe_1 cascade nanozyme. c) Taking advantage of its antisenescence and antioxidant activities, multi-enzyme cascade antioxidant nanozyme can effectively treat atherosclerosis.

catalytic center of GPx for maintaining intracellular redox balance (Se is in the form of selenocysteine in the GPx catalytic center).[17] Considering the essential role of GPx in atherosclerosis,[11d,18] it is reasonable to choose Se for atherosclerosis treatment.[16a] After optimization, Se-doped MIL-53(Fe)-NO_2 (named MSe_1) was able to sequentially scavenge $O_2^{\bullet-}$ and H_2O_2 through the cascade catalytic reaction, which therefore prevented cell senescence, attenuated oxidative stress-induced inflammation, and inhibited oxLDL-induced foam cell formation. *In vivo* therapeutic studies in $ApoE^{-/-}$ mice substantiated that the MSe_1 nanozyme prevented the progression of atherosclerosis by attenuating the senescent cells and suppressing inflammation in atherosclerotic plaques.

Results and Discussion

Synthesis and Characterization of MIL-53(Fe)-X and MIL-53(Fe)-NO_2@Se_x (x = 0.5, 1, 2, and 5)

MIL-53(Fe)-X (X = NH_2, F, OH, NO_2, and H) MOFs were synthesized by assembling iron metal nodes and terephthalate linkers (substituted terephthalate linkers, Figure S1a). The powder X-ray diffraction (PXRD) patterns of MIL-53(Fe)-X MOFs all maintained the crystalline phase and were in accordance with the literature, which indicated the successful synthesis (Figure S1b). Then, the SOD-like activity of MIL-53(Fe)-X was studied by using hydroethidine, an SOD specific probe. Among them, MIL-53(Fe)-NO_2 had the highest SOD-like activity (Figure S1c), so it was selected for further investigation.

To obtain the cascade nanozymes, different contents of Se were added during the synthesis of MIL-53(Fe)-NO_2. The obtained products were named as MSe_x (x = 0.5, 1, 2, and 5, which means the different amounts of Se incorporated). The FT-IR spectra showed that $MSe_{0.5}$, MSe_1, MSe_2, and MSe_5 all maintained the basic structure of MIL-53(Fe)-NO_2, which indicated that the incorporation of Se had negligible effects on the MOFs (Figure S2). Additionally, to confirm the existence of Se, we carried out X-ray photoelectron spectroscopy (XPS) measurements. The full XPS spectra of MSe_x are shown in Figure S3, demonstrating the presence of Se and Fe. In addition, the high-resolution XPS spectra of Se 3*d* demonstrated that the doped Se was mainly in its elemental state. The peak located at around 59.0 eV could be attributed to the oxidization of Se during synthesis and the loss feature of Se metal.

Afterward, we investigated the SOD- and GPx-like activities of $MSe_{0.5}$, MSe_1, MSe_2, and MSe_5. First, the SOD-like activity was investigated by monitoring the $O_2^{\bullet-}$ scavenging efficiency. As shown in Figure 2a, all four nanozymes scavenged most of the $O_2^{\bullet-}$, indicating their excellent SOD-like activity. This is reasonable because the ratios of Fe^{2+}/Fe^{3+} in the four samples were almost equal (Table S1). In contrast, there was an obvious correlation between the GPx-like activity and the content of Se in MSe_x nanozymes (Figure 2b and Figure S4). This is because Se is the active center of the GPx mimics.

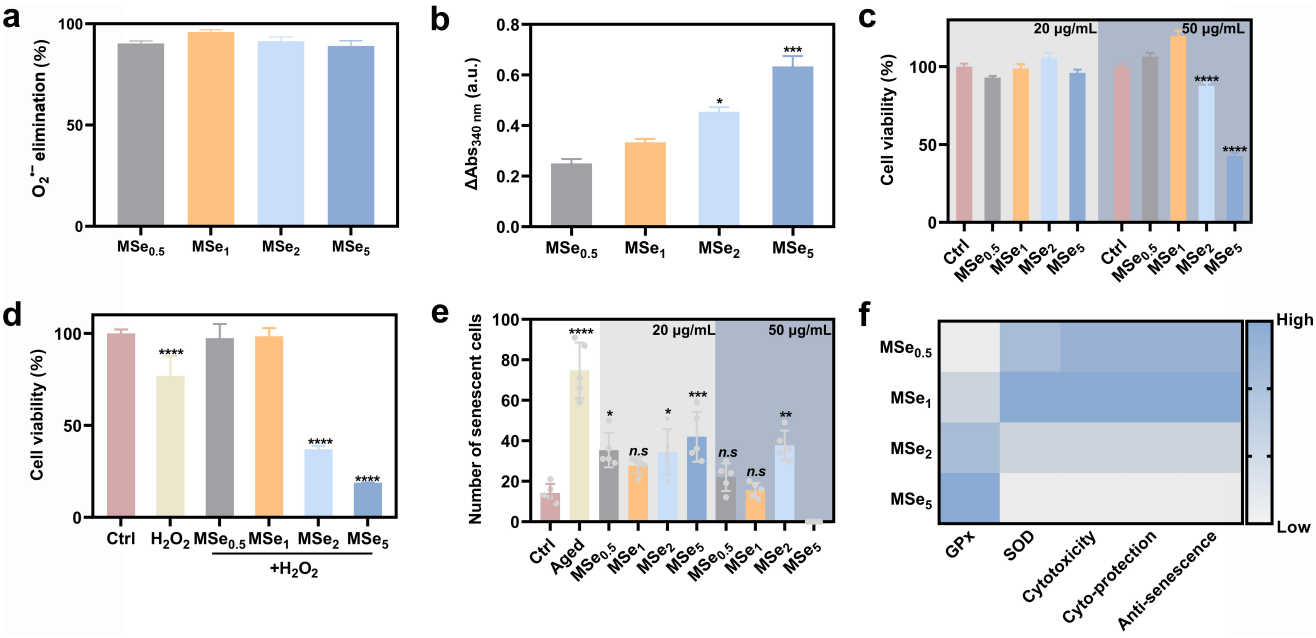

Figure 2. Enzyme mimicking activities and cellular evaluation of MSe_x. a) SOD-like and b) GPx-like activities of MSe_x. Data are presented as mean ± SD (n = 3). Statistical differences were analyzed by one-way ANOVA and Student's t-test: * $p < 0.05$ and *** $p < 0.001$ vs. MSe_1 group. c) Cytotoxicity after treatment with MIL-53(Fe)-NO_2@Se_x at 20 μg/mL and 50 μg/mL. d) Cytoprotective ability of MSe_x. e) Number of senescent cells in culture dish per mm^2. The aged cells were counted based on SA-β-gal staining. Data are presented as mean ± SD (n = 5). Statistical differences were analyzed by one-way ANOVA and Student's t-test: * $p < 0.05$, ** $p < 0.01$, *** $p < 0.001$, **** $p < 0.0001$, and *n.s* (not significant) vs. control group. f) Heat map of the various qualities (antioxidant activity and cellular evaluation) of MSe_x.

After demonstrating the excellent SOD- and GPx-like activity of MSe_x nanozymes, we assessed their cytoprotective effect and biocompatibility. As shown in Figure 2c, after human umbilical vein endothelial cell (HUVEC) was incubated with MSe_x for 24 h at a concentration of 20 μg/mL, all four nanozymes exhibited negligible cytotoxicity. However, at a higher concentration of 50 μg/mL, MSe_2 and MSe_5 had apparent cytotoxicity, especially MSe_5, but the other two had no cytotoxicity. Subsequently, the cell protective ability of the MSe_x nanozymes against oxidative stress induced by H_2O_2 was studied (Figure 2d). Treatment with H_2O_2 significantly decreased cell viability. While $MSe_{0.5}$ and MSe_1 alleviated oxidative stress-induced cell death, both MSe_2 and MSe_5 had poor performance. MSe_2 and MSe_5 decreased the cell viability and even aggravated the cell death. From these results, we found that the more the Se was incorporated, the more the cytotoxicity was caused. The elevated cytotoxicity of MSe_2 and MSe_5 could be attributed to their higher GPx-like activity compared with the other two MSe_x. During the GPx-like catalysis, MSe_x catalytically scavenges H_2O_2 by oxidizing glutathione (GSH) to glutathione disulfide (GSSG). Glutathione reductase then consumes nicotinamide adenine dinucleotide phosphate (NADPH) to catalyze the reduction of GSSG back to GSH. If there are excess GPx-mimics, GSH is overconsumed, NADPH is exhausted, and then the cells die.[19]

We further investigated the antisenescence ability of MSe_x, which is one of the main reasons for its antiatherosclerosis activity. We generated a model of cellular senescence by H_2O_2 (a well-established *in vitro* model of senescent cells) in HUVECs. We evaluated the antisenescence ability by senescence-associated β-galactosidase (SA-β-gal) staining (Figure S5), a biomarker of senescent cells in culture and *in vivo*.[20] As shown in Figure 2e, at a low concentration of 20 μg/mL, except MSe_1, the other nanozymes did not show antisenescence activities. Only the number of senescent cells in the MSe_1-treated group showed no significant difference from that in the control group. At a higher concentration of 50 μg/mL, MSe_5 caused the senescent cell death, while the minimum number of senescent cells appeared after treatment with MSe_1, indicating that the MSe_1 effectively attenuated cellular senescence. After a comprehensive evaluation of the multiple antioxidant activities and cellular efficiency, the MSe_1 nanozyme with simultaneous multiple antioxidant activities, biosafety (good biocompatibility with vascular smooth muscle cells (VSMCs), RAW264.7, and HUVECs, Figure S10), excellent antisenescence, and the cytoprotective effect was proven to be more potent for atherosclerosis therapy (Figure 2f).

MSe_1 Attenuated HUVEC Senescence and Protected Cells from ROS-Induced Oxidative Stress

DNA damage is the primary cause of cellular senescence, where ROS represents the main endogenous culprit.[21] The above investigation has proven that the MSe_1 nanozyme can attenuate the senescence of HUVECs. Then, we explored whether MSe_1 attenuates the senescence of HUVECs through the protection of DNA from damage. First, HUVECs were induced to senescence by using H_2O_2 or lipopolysaccharide (LPS), which was evaluated by the expression of lysosomal SA-β-gal (Figure S11 and Figure S12). It was evident that the amount of SA-β-gal in HUVECs decreased significantly after treatment with the MSe_1 nanozyme, compared to Se treatment, MIL-53(Fe)-NO_2 treatment, and untreated cells. DNA damage can be assessed by phosphorylated H2A histone family member X (γ-H2AX), which forms when double-strand breaks appear. We next assessed the expression of γ-H2AX by immunofluorescence staining. As shown in Figure 3a and Figure S13, the senescent cells displayed a considerably high level of γ-H2AX, while the level of γ-H2AX decreased after MSe_1 but not Se or MIL-53(Fe)-NO_2 treatments (Figure 3d). These results indicated that the MSe_1 nanozyme attenuates HUVEC senescence by protecting DNA from damage. To further confirm the antisenescence activity of MSe_1, the established senescence marker p16(INK4a) (p16), which is correlated positively with senescence, was verified by immunofluorescence staining. The results showed that MSe_1 could significantly attenuate the expression of p16 (Figure 3b, Figure 3e, and Figure S14). These results corroborated the outstanding antisenescence activity of MSe_1 at the *in vitro* level.

Several lines of evidence provide the impetus for investigating cell senescence and ROS.[22] According to the free-radical theory, ROS may be a potential candidate responsible for senescence and oxidative stress.[23] The excessive ROS-induced oxidative stress is closely associated with the pathogenesis of atherosclerosis, which regulates multiple vascular cell functions, such as endothelial cell senescence and the migration of VSMCs. Moreover, the overproduction of ROS and sustained oxidative stress can induce tissue and cell injury that further initiates an inflammatory cycle and amplifies oxidative stress. Therefore, we examined whether MSe_1 could inhibit ROS generation in RAW264.7 macrophages and HUVECs. The two kinds of cells were treated with H_2O_2 or LPS to simulate the overproduction of intracellular ROS. Cells cultured with medium alone served as the normal control. The intracellular ROS scavenging ability of MSe_1 was monitored with an intracellular ROS fluorescent probe, 2′,7′-dichlorofluorescein diacetate (DCFH-DA) (Figure 3c, Figure S15, and Figure S16). Fluorescence microscopy imaging clearly confirmed that the MSe_1 group presented less DCFH-DA fluorescence intensity in cells than the Se and MIL-53(Fe)-NO_2 groups (Figure 3c and Figure 3f). In contrast, the LPS-stimulated group showed the highest fluorescence intensity. These results indicated that MSe_1 scavenged intracellular ROS. The flow cytometry results showed that the ROS scavenging ability of MSe_1 was concentration-dependent (Figure S17). To understand how the MSe_1 nanozyme affects the levels of $O_2^{\bullet-}$, H_2O_2, and hydroxyl radical ($^{\bullet}OH$) inside RAW264.7 cells, their corresponding specific dyes dihydroethidium (DHE), ROSGreen, and hydroxyphenyl fluorescein (HPF) were used for detection. The results showed that MSe_1 could significantly attenuate the levels of $O_2^{\bullet-}$ (Figure S18), H_2O_2 (Figure S19), and $^{\bullet}OH$ (Figure S20) in

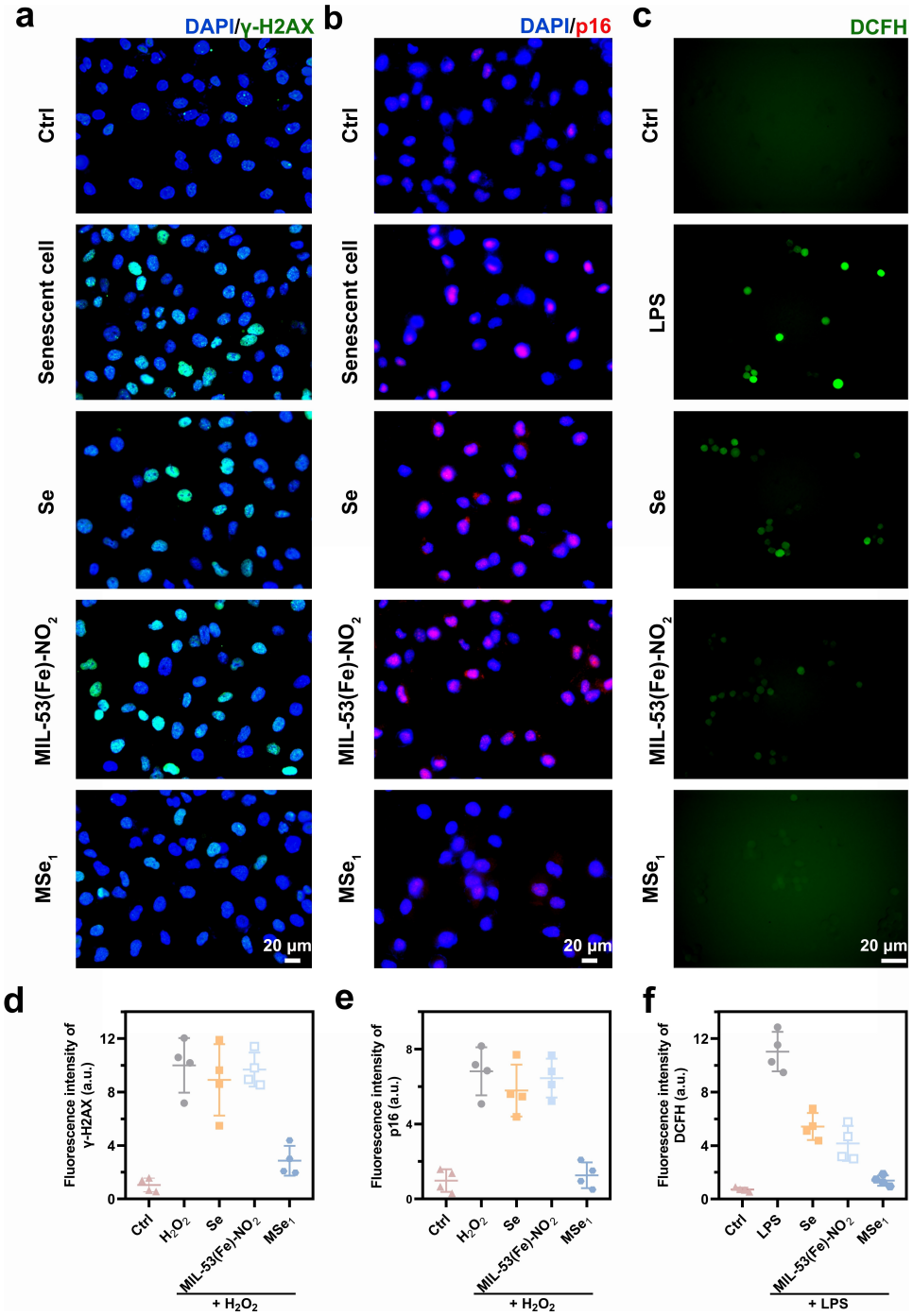

Figure 3. Antisenescence and antioxidant activities of MSe_1. a) DNA damage response in HUVEC senescence models (assessed by anti-γ-H2AX immunofluorescence). b) Antisenescence activity verified by immunofluorescence staining of p16 in HUVEC senescence models. c) Fluorescence microscopy images of ROS levels in RAW264.7 cells under LPS induction. Quantitative analysis of the average optical density of d) γ-H2AX, e) p16, and f) DCFH. Data are presented as mean ± SD ($n=4$). Statistical differences were analyzed by one-way ANOVA and Student's t-test: $^{*}p<0.05$, $^{**}p<0.01$, $^{***}p<0.001$, and $^{****}p<0.0001$ vs. H_2O_2 group.

RAW264.7 cells. Similarly, from the results of flow cytometry, MSe_1 also eliminated LPS- and H_2O_2-induced ROS in HUVECs (Figure S21). These results of cellular experiments proved that the MSe_1 nanozyme with simultaneous multiple antioxidant activities has more power to scavenge overproduced ROS in organisms.

Oxidative stress (H_2O_2 and $O_2^{\bullet-}$) has been indicated to promote VSMC proliferation and migration, which contribute to the initiation and early progression of atherosclerosis. We conducted a wound healing experiment, and the results showed that MSe_1 effectively reduced VSMC migration and proliferation (Figure S22). To this end, MSe_1 had the best

multiple enzyme-like activity, attenuated HUVEC senescence, scavenged ROS in cells, and reduced the migration of VSMCs, which should have great promise in atherosclerosis prevention.

In vitro Inhibition of Cellular Internalization of oxLDL and Foam Cell Formation by MSe_1 Nanozyme

Oxidized low-density lipoprotein (oxLDL), the low-density lipoprotein oxidized by ROS, is an important contributing factor to vascular senescence. OxLDL has several proatherogenic activities, such as promoting foam cell formation and stimulating ROS generation.[24] The formation of foam cells is the hallmark of atherosclerosis lesion development, from initial lesions to advanced plaques. During this process, in addition to macrophage uptake of oxLDL to form foam cells, ECs can also become foam cells.[25] The lipid accumulation in the inner walls of blood vessels caused atherosclerosis.[26] Inhibiting foam cell formation by attenuating oxLDL internalization is a profitable way to prevent and remedy atherosclerosis. Biological studies have indicated that GPx deficiency accelerates atherosclerosis and increases lesion cellularity in $ApoE^{-/-}$ mice by promoting macrophage foam cell formation and proliferation.[11a,27] Therefore, we investigated the effect of MSe_1 nanozyme treatment on the cellular uptake of oxLDL in both RAW264.7 cells and HUVECs. Significant red fluorescence was observed in the cytoplasm of RAW264.7 cells after treatment with DiI-labeled oxLDL (DiI-oxLDL) (Figure 4a and Figure S23). Treatment of macrophages with Se and MIL-53(Fe)-NO_2 did not reduce intracellular uptake of DiI-oxLDL. In contrast, with the same doses of MSe_1, the fluorescence of DiI-oxLDL was notably lower in RAW264.7 macrophages. Furthermore, to confirm this result, flow cytometric analysis was performed to quantify intracellular DiI-oxLDL (Figure 4b). We observed that after pretreatment with the same doses of Se, MIL-53(Fe)-NO_2, and MSe_1, significantly attenuated oxLDL internalization was observed only in the MSe_1 group. The same result was obtained in HUVECs, where MSe_1 effectively inhibited oxLDL uptake in HUVECs (Figure 4c).

Then, we stained the intracellular lipid droplets with oil red O (ORO) and examined whether the MSe_1 nanozyme is effective in inhibiting foam cell formation. Consistent with the studies above, RAW264.7 macrophages treated with oxLDL showed considerable intracellular lipid droplets and significant macrophage foam cell formation (Figure 4d, top panel). Moreover, the number of macrophage foam cells was not reduced following treatment with Se and MIL-53(Fe)-NO_2. However, foam cell formation was significantly inhibited via treatment with MSe_1. Likewise, treatment with the MSe_1 nanozyme reduced foam cells derived from oxLDL-stimulated HUVECs (Figure 4d, bottom panel). The results demonstrated that the cascade nanozyme MSe_1 can attenuate the formation of foam cells from macrophages and HUVECs by reducing the cellular inter-

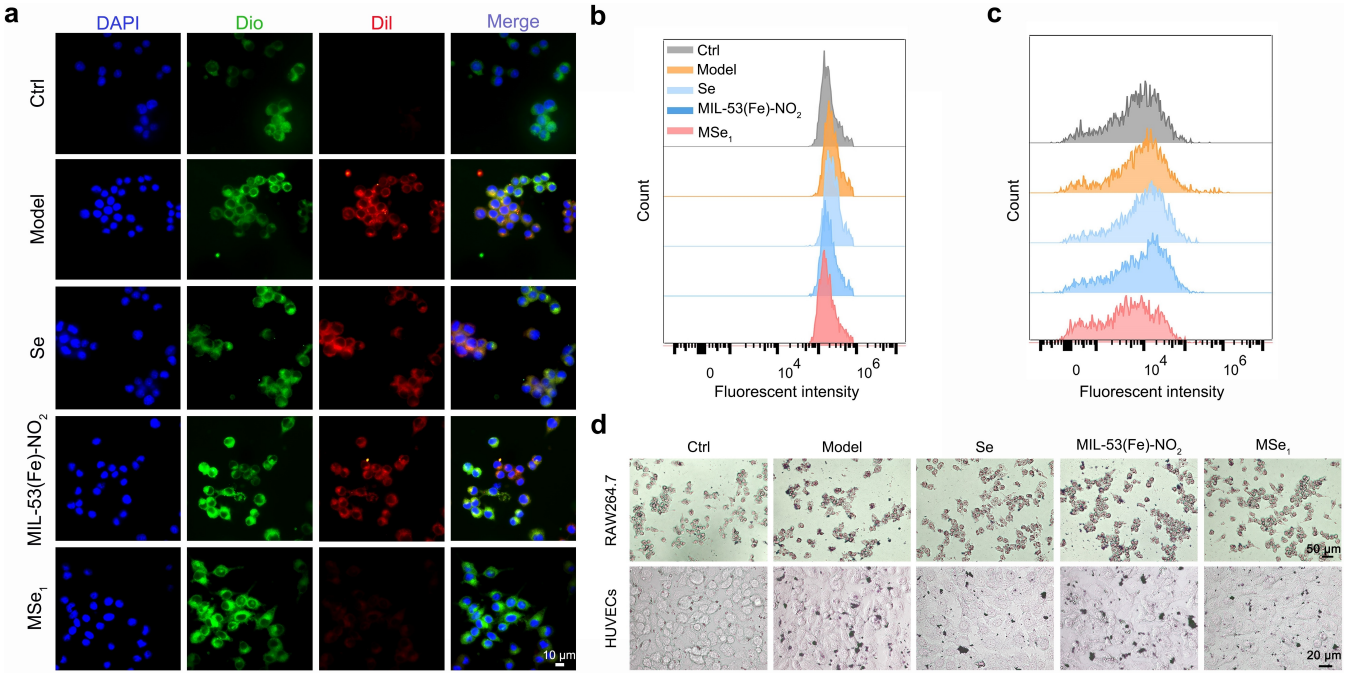

Figure 4. Effect of MSe_1 nanozyme on cellular uptake of oxLDL and foam cell formation in macrophages and HUVECs. a) Confocal fluorescence images showed cellular internalization of DiI-labeled oxidized LDL (DiI-oxLDL) in RAW264.7 cells. After preincubation with fresh medium (the model group) or various nanozymes for 2 h, cells were cultured with DiI-oxLDL for 4 h, followed by confocal microscopic observation and flow cytometric analysis. Cells in the normal control group were not incubated with DiI-oxLDL. For fluorescence observation, nuclei were stained with DAPI (blue), and the cell membrane was labeled with DiO (green). Quantification of intracellular DiI-oxLDL in b) RAW264.7 cells and c) HUVECs was detected by flow cytometry. d) Optical microscopy images showed oxLDL-induced foam cell formation in macrophages and HUVECs.

nalization of oxLDL, exhibiting a competitive advantage over the other nanozymes.

In vivo Treatment of Atherosclerosis by *i.v.*-delivered MSe_1 Nanozymes in $ApoE^{-/-}$ Mice

After confirming the effectiveness of MSe_1 *in vitro*, the *in vivo* therapeutic effects of the MSe_1 nanozyme were examined. $ApoE^{-/-}$ mice were fed a high-fat diet for 2.5 months. After the first month, they were randomly assigned into four groups (5 mice per group). Then, different preparations with the same concentration were administered by *i. v.* injection every three days (Figure 5a). After that, the entire aortas were collected and stained with ORO. As shown in Figure 5b, the saline group showed the largest ORO-positive areas. Treatment with Se and MIL-53(Fe)-NO_2 did not afford significant effects. In

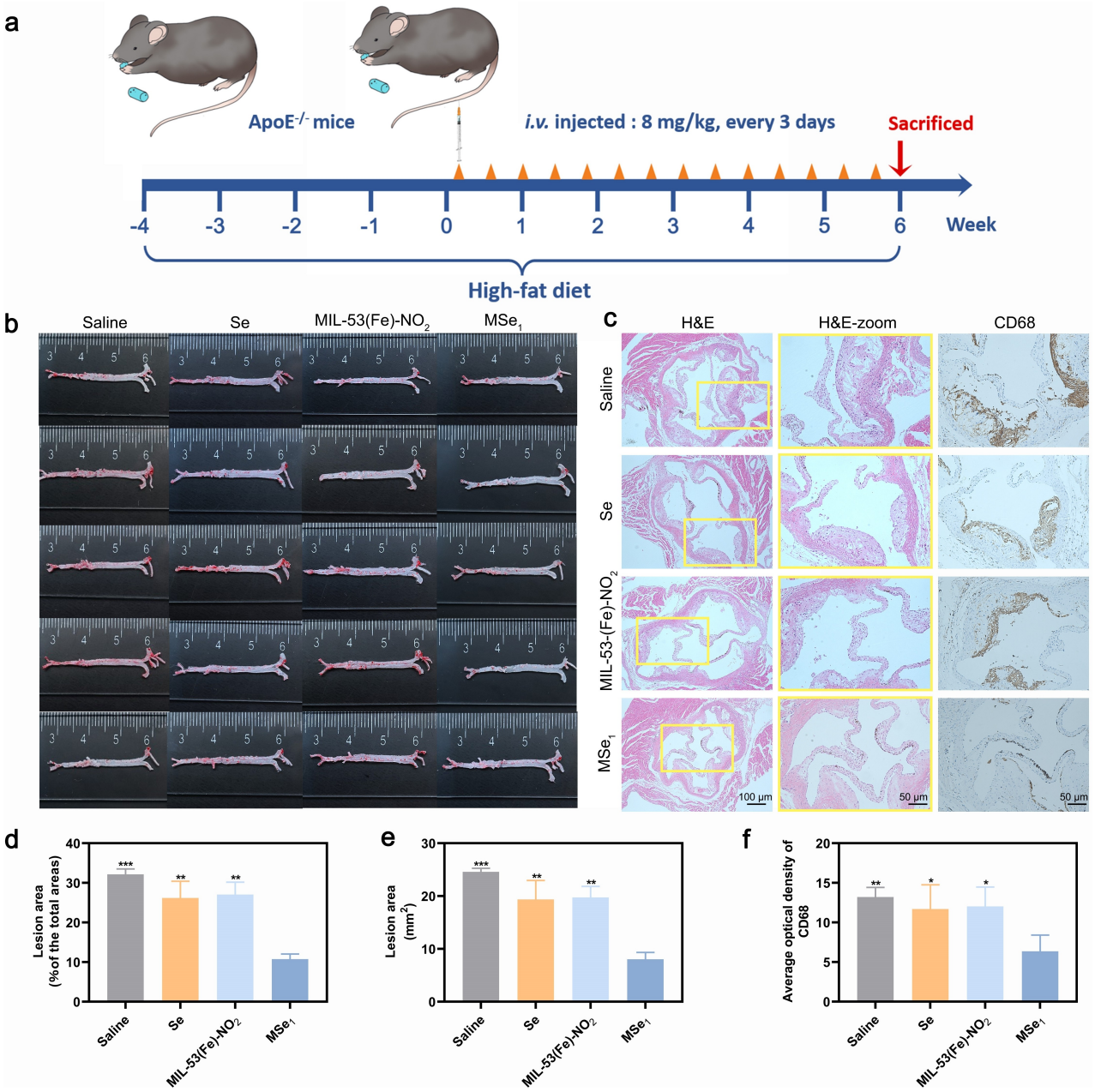

Figure 5. Therapeutic effects of *i.v.*-delivered nanozymes in $ApoE^{-/-}$ mice. a) Schematic illustration of the treatment protocols. b) Photographs of en face ORO-stained whole aortas from $ApoE^{-/-}$ mice after treatment with saline and different nanozymes. c) Representative images of aortic root sections stained with H&E and an antibody against CD68. Scale bar in H&E was 100 μm, and scale bar in H&E-zoom and CD68 were 50 μm. Quantitative analysis of d) the lesion area in aortas, e) the lesion areas of the whole aortas, and f) the average optical density of CD68. Data are presented as mean ± SD ($n = 5$). Statistical differences were analyzed by one-way ANOVA and Student's t-test: $^{*}p < 0.05$, $^{**}p < 0.01$, $^{***}p < 0.001$, and $^{****}p < 0.0001$ vs. MSe_1 group.

contrast, after treatment with MSe_1, much fewer ORO-stained areas were observed. On the basis of the above results, we conducted further quantification. The quantification results indicated that the average plaque area was 32.16 ± 3.08, 28.20 ± 4.50, 27.03 ± 4.02, and 10.75 ± 2.93 % for $ApoE^{-/-}$ mice treated with saline, Se, MIL-53(Fe)-NO_2, and MSe_1 nanozyme, respectively (Figure 5d). Meanwhile, there were significant differences between the MSe_1 group and the Se or MIL-53(Fe)-NO_2 group (Figure 5d and 5e). To better understand the composition of atherosclerotic plaques, sections of the aortic sinus were analyzed by histochemistry. In accordance with immunofluorescence and hematoxylin/eosin (H&E) staining, we found that plaques in the saline group primarily consisted of acellular and lipid-rich necrotic cores (Figure 5c). However, the necrotic core area was significantly lower after MSe_1 nanozyme therapy than that of the saline and the other two groups. The CD68 was stained to evaluate the macrophage count. In the saline group, high CD68 positivity was obtained in the plaques. After administration of MSe_1, the expression of CD68 was much lower. However, there was no difference in the Se and MIL-53(Fe)-NO_2 groups compared with the saline group (Figure 5f). These findings confirmed that the cascade nanozyme MSe_1 exhibited superior therapeutic efficacy, which could more effectively inhibit the progression of atherosclerosis and suppress luminal narrowing due to the blockade of macrophage infiltration.

MSe_1 Nanozyme Achieves Therapeutic Effect by Attenuating Cellular Senescence and Cascade ROS Scavenging

Collagen surrounding plaques is closely related to plaque stability.[26b,28] The high level of collagen in atherosclerotic plaques indicates plaque stability.[29] Next, we detected the content of collagen in plaque areas using Masson's trichrome staining (Figure 6a and Figure S24a). With MSe_1 therapy, the collagen in the plaque and the fibrous cap thickness were significantly enhanced (Figure 6d). Separate staining with anti-matrix metalloproteinase-9 (MMP-9) antibody indicated that MSe_1 therapy effectively reduced MMP-9 expression in plaques (Figure S25). Because MMP-9 expression is positively related to plaque vulnerability, the results demonstrated that MSe_1 therapy could more effectively stabilize atherosclerotic plaques. These results, together with the decreased necrotic core area and macrophages, demonstrated that the *i. v.* treatment with the MSe_1 nanozyme can efficaciously stabilize atherosclerotic plaques.

Then, the mechanisms responsible for the *in vivo* antiatherosclerosis activity of the MSe_1 nanozyme were determined. Attenuating cellular senescence in early lesions holds promise for the treatment of atherosclerosis.[5] The results of staining with γ-H2AX antibody indicated that MSe_1 nanozyme treatment effectively reduced senescent cells in plaque areas (Figure 6b, 6e and Figure S24b), while the other three groups displayed more bright green fluorescence. Senescence *in vivo* was also verified by IF staining with p16, another established senescence marker. The results showed that the expression of p16 is very low

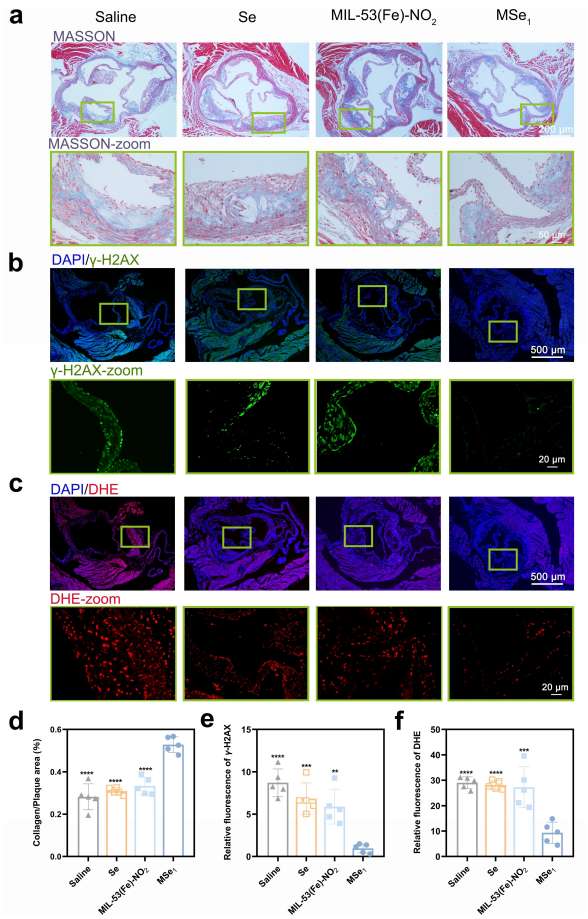

Figure 6. Histochemistry analyses of aortic root sections from $ApoE^{-/-}$ mice after different treatments. Representative images of aortic root sections stained with a) Masson's trichrome, b) an antibody against γ-H2AX (green), and c) DHE fluorescent probe (red). DAPI for nucleus (blue). Quantitative analysis of d) plaque collagen area relative to plaque area and average fluorescence of e) γ-H2AX- and f) DHE-stained aortic root sections from $ApoE^{-/-}$ mice after different treatments. Data are presented as mean $\pm$ SD ($n = 5$). Statistical differences were analyzed by one-way ANOVA and Student's t-test: $^{**}p < 0.01$, $^{***}p < 0.001$, and $^{****}p < 0.0001$ vs. MSe_1 group.

after MSe_1 nanozyme treatment (Figure S26). This was the same as the result of γ-H_2AX. This is consistent with the relationship between cellular senescence and oxidative stress that we have shown above. Then, superoxide production was detected by DHE staining (Figure 6c and Figure S24c). DHE-stained sections of aortic roots from $ApoE^{-/-}$ mice in the saline-treated group show a high level of red fluorescence due to DHE with superoxide anions yielding ethidium with red fluorescence. The red fluorescence of the MSe_1 nanozyme group was significantly lower than that of the other groups (Figure 6f). The results showed that oxidative stress was significantly mitigated by *i. v.*-delivered MSe_1 nanozyme. Accordingly, these results demonstrated that the MSe_1 nanozyme could effectively attenuate systemic oxidative stress and senescent cells in plaques.

Biosafety Assessment

To assess the biosafety of MSe_1, the levels of typical hematological parameters after MSe_1 injection at different doses were first determined. With injections of MSe_1, the complete blood count in C57BL/6J mice implied that the levels of red blood cells, white blood cells, platelets, and hemoglobin were in normal ranges (Figure S27). Then, we investigated the safety evaluations in $ApoE^{-/-}$ mice after long-term treatment with different formulations. There was no significant difference in the body weight of mice among the various treatment groups (Figure S28). After long-term treatment, compared to the saline and other two groups, the MSe_1 groups displayed lower levels of triglyceride (TG) and LDL, whereas no significant changes in total cholesterol (CHO) and high-density lipoprotein (HDL) were found (Figure S29). Moreover, these parameters did not change after treatment with MSe_1 in C57BL/6J mice (Figure S30). These results showed that the injection of MSe_1 did not change the blood lipid level of the mice themselves. Next, we examined H&E-stained histological sections of major organs (heart, liver, spleen, lung, and kidney). None of the experimental groups showed apparent toxicity (Figure S31). Accordingly, the above results suggested that *i.v.* administration of the MSe_1 nanozyme is safe at the examined dose. Finally, the biodistribution of Se and Fe, the main elements of MSe_1, was examined in the heart, liver, spleen, lung, and kidney. By inductively coupled plasma optical emission spectrometer (ICP-OES), we found that Fe and Se were mainly distributed in the spleen and liver (Figure S32). However, the accumulation was not significantly higher, and the data indicated that the nanozymes were not inclined to accumulate in vital organs, revealing the biosafety of the MSe_1 nanozyme.

Conclusion

A cascade nanozyme MSe_1 with antisenescence and ROS-scavenging activities was successfully synthesized by incorporating Se into MIL-53(Fe)-NO_2 MOF. The MSe_1 nanozyme with SOD- and GPx-like abilities was able to scavenge various radicals and attenuate cellular senescence effectively. By eliminating overproduced intracellular ROS, the MSe_1 nanozyme effectively inhibited ROS-induced inflammatory responses in macrophages and HUVECs. By protecting DNA from damage, the MSe_1 nanozyme attenuated HUVEC senescence, which is one of the key drivers of atherosclerosis formation and maturation. Moreover, the MSe_1 nanozyme significantly decreased the cellular uptake of oxLDL, thereby suppressing foam cell formation in macrophages and HUVECs. After *i.v.* injection, the MSe_1 nanozyme effectively delayed the development of atherosclerosis in $ApoE^{-/-}$ mice. This work not only provides guidance for developing nanozymes with multiple antioxidant activities but also demonstrates that increased activity and cascade construction can reduce the dose of therapeutic nanozymes. Consequently, it will broaden the potential of nanozymes in biomedical applications.

Acknowledgements

This work was supported by the National Key R&D Program of China (2019YFA0709200 and 2021YFF1200700), the National Natural Science Foundation of China (21874067 and 21722503), the PAPD Program, the Jiangsu Provincial Key R&D Program (BE2022836) and Fundamental Research Funds for the Central Universities (202200325).

Conflict of Interest

The authors declare no conflict of interest.

Data Availability Statement

The data that support the findings of this study are available from the corresponding author upon reasonable request.

Keywords: Atherosclerosis · Metal-Organic Framework · Nanozyme · Reactive Oxygen Species (ROS) · Senescent Cell

[1] V. Gorgoulis, P. D. Adams, A. Alimonti, D. C. Bennett, O. Bischof, C. Bishop, J. Campisi, M. Collado, K. Evangelou, G. Ferbeyre, J. Gil, E. Hara, V. Krizhanovsky, D. Jurk, A. B. Maier, M. Narita, L. Niedernhofer, J. F. Passos, P. D. Robbins, C. A. Schmitt, J. Sedivy, K. Vougas, T. von Zglinicki, D. Zhou, M. Serrano, M. Demaria, *Cell* **2019**, *179*, 813–827.

[2] M. S. Chen, R. T. Lee, J. C. Garbern, *Cardiovasc. Res.* **2022**, *118*, 1173–1187.

[3] a) S. I. Bloom, M. T. Islam, L. A. Lesniewski, A. J. Donato, *Nat. Rev. Cardiol.* **2023**, *20*, 38–51; b) N. Basisty, A. Kale, O. H. Jeon, C. Kuehnemann, T. Payne, C. Rao, A. Holtz, S. Shah, V. Sharma, L. Ferrucci, J. Campisi, B. Schilling, *PLoS Biol.* **2020**, *18*, e3000599.

[4] J. L. M. Björkegren, A. J. Lusis, *Cell* **2022**, *185*, 1630–1645.

[5] B. G. Childs, D. J. Baker, T. Wijshake, C. A. Conover, J. Campisi, J. M. van Deursen, *Science* **2016**, *354*, 472–477.

[6] A. J. Donato, R. G. Morgan, A. E. Walker, L. A. Lesniewski, *J. Mol. Cell. Cardiol.* **2015**, *89*, 122–135.

[7] a) Z. S. Chang, J. B. Xia, H. Y. Wu, W. T. Peng, F. Q. N. Jiang, J. Li, C. Q. Liang, H. Zhao, K. S. Park, G. H. Song, S. K. Kim, R. J. Huang, L. Zheng, D. Q. Cai, X. F. Qi, *Aging Cell* **2019**, *18*, e12990; b) R. M. Touyz, A. Anagnostopoulou, L. D. Camargo, A. C. Montezano, *Circ. Res.* **2016**, *119*, 969–971.

[8] B. G. Childs, M. Durik, D. J. Baker, J. M. van Deursen, *Nat. Med.* **2015**, *21*, 1424–1435.

[9] a) U. Forstermann, W. C. Sessa, *Eur. Heart J.* **2012**, *33*, 829–837; b) S. W. Ballinger, C. Patterson, C. A. Knight-Lozano, D. L. Burow, C. A. Conklin, Z. Hu, J. Reuf, C. Horaist, R. Lebovitz, G. C. Hunter, K. McIntyre, M. S. Runge, *Circulation* **2002**, *106*, 544–549.

[10] E. Lubos, J. Loscalzo, D. E. Handy, *Antioxid. Redox Signaling* **2011**, *15*, 1957–1997.

[11] a) F. Cheng, M. Torzewski, A. Degreif, H. Rossmann, A. Canisius, K. J. Lackner, *PLoS One* **2013**, *8*, e72063; b) Y. Li, T. T. Huang, E. J. Carlson, S. Melov, P. C. Ursell, J. L. Olson, L. J. Noble, M. P. Yoshimura, C. Berger, P. H. Chan, D. C. Wallace, C. J. Epstein, *Nat. Genet.* **1995**, *11*, 376–381; c) S. Blankenberg, H. J. Rupprecht, C. Bickel, M. Torzewski, G.

Hafner, L. Tiret, M. Smieja, F. Cambien, J. Meyer, K. J. Lackner, I. AtheroGene, *N. Engl. J. Med.* **2003**, *349*, 1605–1613; d) P. Lewis, N. Stefanovic, J. Pete, A. C. Calkin, S. Giunti, V. Thallas-Bonke, K. A. Jandeleit-Dahm, T. J. Allen, I. Kola, M. E. Cooper, J. B. de Haan, *Circulation* **2007**, *115*, 2178–2187; e) M. Torzewski, V. Ochsenhirt, A. L. Kleschyov, M. Oelze, A. Daiber, H. Li, H. Rossmann, S. Tsimikas, K. Reifenberg, F. Cheng, H. A. Lehr, S. Blankenberg, U. Forstermann, T. Munzel, K. J. Lackner, *Arterioscler. Thromb. Vasc. Biol.* **2007**, *27*, 850–857.

[12] a) L. Z. Gao, J. Zhuang, L. Nie, J. B. Zhang, Y. Zhang, N. Gu, T. H. Wang, J. Feng, D. L. Yang, S. Perrett, X. Yan, *Nat. Nanotechnol.* **2007**, *2*, 577–583; b) B. W. Liu, Z. Y. Sun, P. J. J. Huang, J. W. Liu, *J. Am. Chem. Soc.* **2015**, *137*, 1290–1295; c) J. J. X. Wu, X. Y. Wang, Q. Wang, Z. P. Lou, S. R. Li, Y. Y. Zhu, L. Qin, H. Wei, *Chem. Soc. Rev.* **2019**, *48*, 1004–1076; d) H. Wei, L. Z. Gao, K. L. Fan, J. W. Liu, J. Y. He, X. G. Qu, S. J. Dong, E. K. Wang, X. Y. Yan, *Nano Today* **2021**, *40*, 101269.

[13] a) W. Zhang, S. L. Hu, J. J. Yin, W. W. He, W. Lu, M. Ma, N. Gu, Y. Zhang, *J. Am. Chem. Soc.* **2016**, *138*, 5860–5865; b) M. Ma, Z. Liu, N. Gao, Z. Pi, X. Du, J. Ren, X. Qu, *J. Am. Chem. Soc.* **2020**, *142*, 21702–21711.

[14] a) Q. Wang, C. Cheng, S. Zhao, Q. Liu, Y. Zhang, W. Liu, X. Zhao, H. Zhang, J. Pu, S. Zhang, H. Zhang, Y. Du, H. Wei, *Angew. Chem. Int. Ed.* **2022**, *61*, e202201101; b) X. Y. Wang, X. J. J. Gao, L. Qin, C. D. Wang, L. Song, Y. N. Zhou, G. Y. Zhu, W. Cao, S. C. Lin, L. Q. Zhou, K. Wang, H. G. Zhang, Z. Jin, P. Wang, X. F. Gao, H. Wei, *Nat. Commun.* **2019**, *10*, 704.

[15] Y. Liu, Y. Cheng, H. Zhang, M. Zhou, Y. Yu, S. Lin, B. Jiang, X. Zhao, L. Miao, C. W. Wei, Q. Liu, Y. W. Lin, Y. Du, C. J. Butch, H. Wei, *Sci. Adv.* **2020**, *6*, eabb2695.

[16] a) Z. Z. Wang, J. X. Wu, J. J. Zheng, X. M. Shen, L. Yan, H. Wei, X. F. Gao, Y. L. Zhao, *Nat. Commun.* **2021**, *12*, 6866; b) J. Wu, Z. Z. Wang, X. Jin, S. Zhang, T. Li, Y. H. Zhang, H. Xing, Y. Yu, H. G. Zhang, X. F. Gao, H. Wei, *Adv. Mater.* **2021**, *33*, 2005024.

[17] a) M. P. Rayman, *Lancet* **2012**, *379*, 1256–1268; b) X. Huang, X. M. Liu, Q. A. Luo, J. Q. Liu, J. C. Shen, *Chem. Soc. Rev.* **2011**, *40*, 1171–1184; c) G. Mugesh, H. B. Singh, *Chem. Soc. Rev.* **2000**, *29*, 347–357; d) Y. Y. Huang, E. Z. Su, J. S. Ren, X. G. Qu, *Nano Today* **2021**, *38*, 101205; e) K. P. Bhabak, G. Mugesh, *Acc. Chem. Res.* **2010**, *43*, 1408–1419.

[18] P. Chew, D. Y. C. Yuen, P. Koh, N. Stefanovic, M. A. Febbraio, I. Kola, M. E. Cooper, J. B. de Haan, *Arterioscler. Thromb. Vasc. Biol.* **2009**, *29*, 823–830.

[19] D. Bhowmick, S. Srivastava, P. D′Silva, G. Mugesh, *Angew. Chem. Int. Ed.* **2015**, *54*, 8449–8453.

[20] F. Debacq-Chainiaux, J. D. Erusalimsky, J. Campisi, O. Toussaint, *Nat. Protoc.* **2009**, *4*, 1798–1806.

[21] a) L. Wu, J. R. Sowers, Y. Zhang, J. Ren, *Cardiovasc. Res.* **2023**, *119*, 691–709; b) S. P. Jackson, J. Bartek, *Nature* **2009**, *461*, 1071–1078.

[22] a) C. Lopez-Otin, M. A. Blasco, L. Partridge, M. Serrano, G. Kroemer, *Cell* **2023**, *186*, 243–278; b) A. R. J. Young, L. D. Cassidy, M. Narita, *Adv. Cancer Res.* **2021**, *150*, 113–145.

[23] a) D. Harrison, K. K. Griendling, U. Landmesser, B. Hornig, H. Drexler, *Am. J. Cardiol.* **2003**, *91*, 7A-11A; b) T. Hayashi, H. Matsui-Hirai, A. Miyazaki-Akita, A. Fukatsu, J. Funami, Q. F. Ding, S. Kamalanathan, Y. Hattori, L. J. Ignarro, A. Iguchi, *Proc. Natl. Acad. Sci. USA* **2006**, *103*, 17018–17023.

[24] a) I. Tabas, K. J. Williams, J. Boren, *Circulation* **2007**, *116*, 1832–1844; b) K. J. Moore, F. J. Sheedy, E. A. Fisher, *Nat. Rev. Immunol.* **2013**, *13*, 709–721; c) L. Z. Huang, K. L. Chambliss, X. F. Gao, I. S. Yuhanna, E. Behling-Kelly, S. Bergaya, M. Ahmed, P. Michaely, K. Luby-Phelps, A. Darehshouri, L. Xu, E. A. Fisher, W. P. Ge, C. Mineo, P. W. Shaul, *Nature* **2019**, *569*, 565–569.

[25] a) Y. Zhao, M. Pennings, R. B. Hildebrand, D. Ye, L. Calpe-Berdiel, R. Out, M. Kjerrulf, E. Hurt-Camejo, A. K. Groen, M. Hoekstra, W. Jessup, G. Chimini, T. J. C. Van Berkel, M. Van Eck, *Circ. Res.* **2010**, *107*, e20–31; b) L. Nagy, P. Tontonoz, J. G. A. Alvarez, H. W. Chen, R. M. Evans, *Cell* **1998**, *93*, 229–240; c) D. A. Chistiakov, A. A. Melnichenko, V. A. Myasoedova, A. V. Grechko, A. N. Orekhov, *J. Mol. Med.* **2017**, *95*, 1153–1165.

[26] a) J. Ouyang, A. Xie, J. Zhou, R. C. Liu, L. Q. Wang, H. J. Liu, N. Kong, W. Tao, *Chem. Soc. Rev.* **2022**, *51*, 4996–5041; b) W. Chen, M. Schilperoort, Y. H. Cao, J. J. Shi, I. Tabas, W. Tao, *Nat. Rev. Cardiol.* **2022**, *19*, 228–249.

[27] Z. Guo, H. Van Remmen, H. Yang, X. Chen, J. Mele, J. Vijg, C. J. Epstein, Y. S. Ho, A. Richardson, *Arterioscler. Thromb. Vasc. Biol.* **2001**, *21*, 1131–1138.

[28] a) W. Tao, A. Yurdagul, N. Kong, W. L. Li, X. B. Wang, A. C. Doran, C. Feng, J. Q. Wang, M. A. Islam, O. C. Farokhzad, I. Tabas, J. J. Shi, *Sci. Transl. Med.* **2020**, *12*, eaay1063; b) X. G. Huang, C. Liu, N. Kong, Y. F. Xiao, A. Yurdagul, I. Tabas, W. Tao, *Nat. Protoc.* **2022**, *17*, 748–780.

[29] a) E. F. Rocnik, B. M. Chan, J. G. Pickering, *J. Clin. Invest.* **1998**, *101*, 1889–1898; b) K. Sakakura, M. Nakano, F. Otsuka, E. Ladich, F. D. Kolodgie, R. Virmani, *Heart Lung Circ.* **2013**, *22*, 399–411.

Manuscript received: March 28, 2023
Accepted manuscript online: June 20, 2023
Version of record online: July 4, 2023